IOP Publishing Journal of Physics: Condensed Matter

J. Phys.: Condens. Matter **23** (2011) 234122 (9pp) doi:10.1088/0953-8984/23/23/234122

Dynamic arrest of colloids in porous environments: disentangling crowding and confinement

Jan Kurzidim[1], Daniele Coslovich[2] and Gerhard Kahl[1]

[1] Institut für Theoretische Physik and Center for Computational Materials Science (CMS), Technische Universität Wien, Wien, Austria
[2] Laboratoire Charles Coulomb UMR 5221, Université Montpellier 2 and CNRS, Montpellier, France

E-mail: kurzidim@cmt.tuwien.ac.at

Received 5 December 2010, in final form 25 January 2011
Published 25 May 2011
Online at stacks.iop.org/JPhysCM/23/234122

Abstract
Using numerical simulations we study the slow dynamics of a colloidal hard-sphere fluid adsorbed in a matrix of disordered hard-sphere obstacles. We calculate separately the contributions to the single-particle dynamic correlation functions due to free and trapped particles. The separation is based on a Delaunay tessellation to partition the space accessible to the centres of fluid particles into percolating and disconnected voids. We find that the trapping of particles into disconnected voids of the matrix is responsible for the appearance of a nonzero long-time plateau in the single-particle intermediate scattering functions of the full fluid. The subdiffusive exponent z, obtained from the logarithmic derivative of the mean squared displacement, is essentially unaffected by the motion of trapped particles: close to the percolation transition, we determined $z \simeq 0.5$ for both the full fluid and the particles moving in the percolating void. Notably, the same value of z is found in single-file diffusion and is also predicted by mode-coupling theory along the diffusion–localization line. We also reveal subtle effects of dynamic heterogeneity in both the free and the trapped component of the fluid particles, and discuss microscopic mechanisms that contribute to this phenomenon.

(Some figures in this article are in colour only in the electronic version)

1. Introduction

As colloidal fluid particles move within the external, random field induced by a quenched, disordered arrangement of particles ('matrix'), they can be either hindered in their motion by so-called cages formed by other fluid (mobile) particles, or trapped by the immobile particles of the matrix. In the former case, these cages eventually open due to the steady, collective motion of the fluid, while in the latter case whether or not a fluid particle can escape a certain region of space depends only on pre-set geometric and/or energetic restrictions. Each of these processes alone as well as their interplay are responsible for slowing down the dynamics of the fluid, thereby leading to a complex dynamic behaviour of the system.

These observations represent yet another confirmation that the properties of a fluid that is exposed to a random porous matrix differ substantially from those of a bulk fluid. While these phenomena have been extensively studied in experiment for a wide variety of systems (e.g. [1–6]), related activities in theory and computer simulations lag behind considerably. This discrepancy is mainly due to two problems: (i) a realistic parametrization of typical matrices studied in experiment is very difficult; and (ii) the evaluation of the physical properties of the fluid particles is conceptually difficult and numerically expensive. As a consequence, so far most of the theoretical and simulation-based studies have focused on static structural [7–10], and thermodynamic properties [11–14, 10, 15]. Only during the past few years have investigations on the dynamic properties of such systems come within reach [16–19].

Recently, a major breakthrough has been achieved in the realm of theory: using concepts from the statistical-mechanical description of so-called 'quenched–annealed' (QA) mixtures (see below), a framework has been put forward that allows

the determination of dynamic correlation functions of fluids confined in a porous matrix [20–22]. The theory represents an extension of mode-coupling theory (MCT) [23], a successful framework that can be used to obtain the dynamic correlation functions of a system solely from knowledge about its static structure functions. We shall henceforth refer to the theory as 'ROZ-MCT', owing to the fact that it is based on mathematical methods used in deriving the replica Ornstein–Zernike (ROZ) equations [24], and that it can use structural information provided by the ROZ equations as a source of input.

Meanwhile, thanks to the considerably increased computational power of present-day computers, it is possible to systematically investigate the slow dynamic properties of fluids confined in a disordered environment in computer models. Simulating such systems is costly for multiple reasons: (i) long simulations are necessary to reveal the dynamic slowing-down of dense systems; (ii) a large body of system parameter combinations needs to be considered; and (iii) many independent realizations of the same system have to be generated. The latter requirement arises from the prescription to evaluate the physical properties of QA systems, which involves an explicit double average procedure: the first average is the usual thermodynamic one to be taken over all possible configurations of fluid particles given a fixed matrix configuration; the second average is a disorder average to be performed over all possible matrix representations fulfilling pre-imposed criteria.

Thus far, the ROZ-MCT framework has been applied only to a limited number of models, among which QA systems of hard spheres play a prominent role. In the latter systems, a fluid of hard spheres is confined in a hard-sphere matrix, and cases have been considered in which the fluid and the matrix particles are identical [20–22] or differ in diameter [25]. Within the QA model, a matrix configuration is obtained by taking a snapshot of an equilibrated fluid (quenched component); subsequently the particles of the fluid (annealed component) are immersed in this configuration. Shortly after publication of the theoretical predictions, extensive and systematic molecular dynamics (MD) simulations have been performed for precisely this system [25–27]. While simulations confirmed most of the intriguingly complex features that the theory predicted for the kinetic diagram (such as a discontinuous and a continuous glass transition as well as a continuous diffusion–localization transition), others are yet to be found (in particular the re-entrant glass transition scenario). In this context, it is worth mentioning other recent works which investigate the dynamics of a fluid [18, 19, 28] or of tracer particles [29–32] moving in a matrix of quenched particles.

Our previous work [25, 26] was dedicated to an 'overall' investigation of the dynamic properties (in terms of both single-particle and collective dynamic properties) of hard spheres confined in a disordered matrix of hard-sphere particles, and to a comparison of these results to the theoretical predictions [20–22]. Computer simulations offer the distinct possibility to proceed one step further: in contrast to the theoretical framework, in simulations it is possible to distinguish between caging and trapping by geometrically analysing the voids formed by the matrix particles.

The pertinent procedure reads as follows. Given a particular realization of a state point, the first step is to classify the voids formed by the matrix particles while disregarding the fluid particles. The algorithm used is detailed in [33]; in short, we distinguish between disconnected voids of finite volume from which—due to geometric restrictions—particles cannot escape, and the percolating void that—taking into account the periodic boundary conditions—extends over the entire space and in which particles can propagate infinitely far. (Note that multiple percolating voids can only exist in systems of finite size.) In the second step, for each fluid particle in the system realization we use this void analysis to determine in which class of void the particle is located. The fluid particles thus fall in two classes: 'trapped' particles (superscript 'trap') that populate the disconnected voids, and 'free' particles (superscript 'free') that move in the percolating void. We then compute a set of single-particle dynamic correlation functions (namely the self-intermediate scattering function $F_s(k,t)$, the mean squared displacement $\delta r^2(t)$, and the self-part of the direction-averaged van Hove function $G_s(r,t)$) separately for the trapped and the free particles (i.e., $F_s^{\rm trap}(k,t)$ and $F_s^{\rm free}(k,t)$, etc).

In an effort to specify and to quantify the respective contributions of trapped and free particles to the dynamic structure, $F_s(k,t)$ and $\delta r^2(t)$ are discussed along two specific pathways in the system's parameter space. The latter is spanned by the packing fraction of the fluid, ϕ_f, and that of the matrix, ϕ_m. The properties of $G_s(r,t)$ for the trapped and the free particles are discussed for selected state points in the (ϕ_m, ϕ_f) plane.

Notwithstanding the presentation of quantitative results in section 3, it is worth clarifying what qualitative behaviour should be expected for the dynamic correlation functions. In the long-time limit, the contributions of the trapped and the free particles differ markedly, which bears physical significance. While the single-particle intermediate scattering function of the free particles will always relax completely for $t \to \infty$, this is never the case for $F_s^{\rm trap}(k,t)$. On the other hand, the mean squared displacement of the free particles will always recover diffusive behaviour while $\delta r^2_{\rm trap}(t)$ will always saturate as $t \to \infty$, with the limiting value reflecting the average pore size. Finally, for the free particles the self-part of the van Hove function will rapidly relax towards zero for distances in the vicinity of zero. Conversely, $G_s^{\rm trap}(r \simeq 0, t)$ will decay to a value significantly above zero. Instead, it will approach a steady-state distribution that reflects the distribution in trap sizes and shapes.

The paper is organized as follows. In section 2 we briefly summarize the model and our simulation technique (referencing previous publications for more details). Section 3 is dedicated to the results; after a brief summary of our void identification algorithm as well as a short discussion of the void analysis of the state points treated in this contribution, we present in detail our results for the single-particle correlation functions. In section 4 we discuss implications of those results, and present explanations for the observations. The paper is closed with concluding remarks.

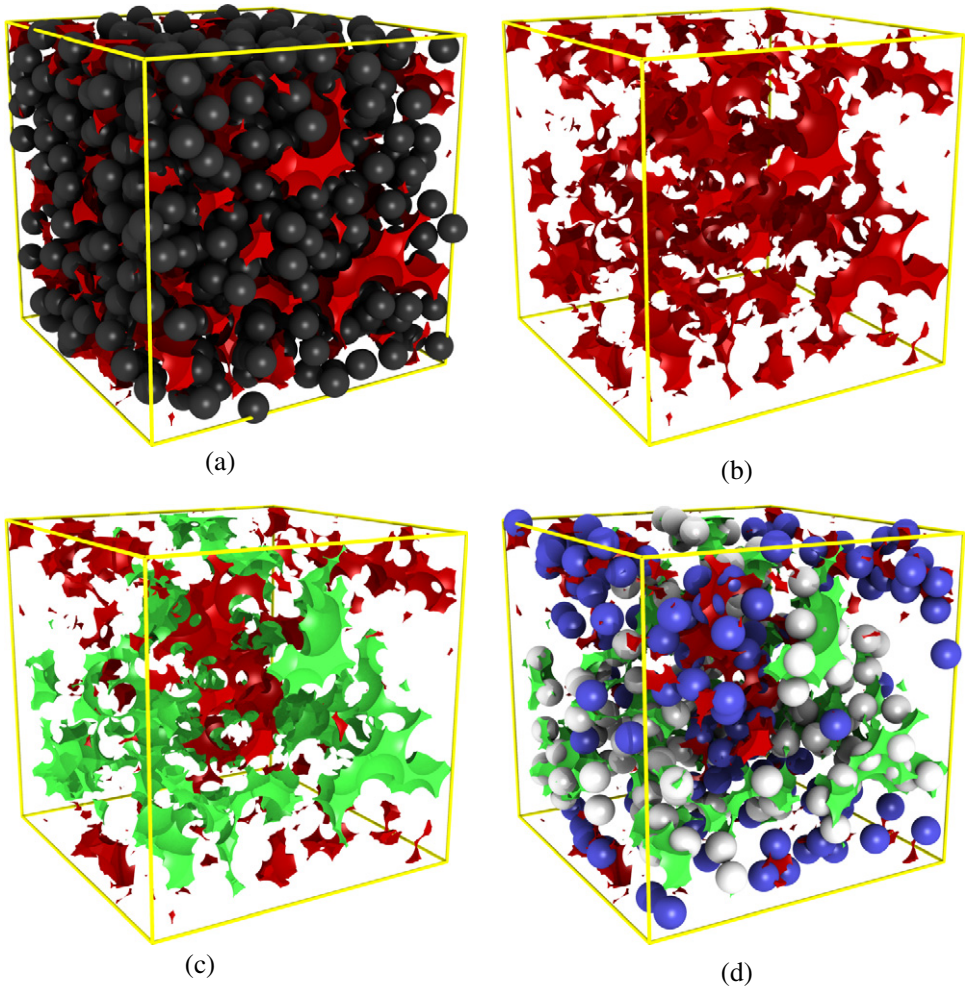

Figure 1. Visualization of the procedure to identify trapped and free fluid particles. (a) Dark (grey) spheres: matrix particles. Volumes in lighter (red) shade: voids (volumes accessible to the centers of the fluid particles). (b) Same as previous, with the matrix particles removed. (c) Same as previous, with the percolating void highlighted in a light (green) shade. (d) Same as previous, with a sample set of fluid particles inserted into the voids. Light (grey) spheres: free particles. Dark (blue) spheres: trapped particles.

2. Model and theoretical approaches

Following our previous work, we have used the QA protocol to describe the properties of fluid particles that are exposed to an external field of a random porous matrix. In this picture, the fluid particles move within the space left free by the matrix: both types of particles interact with each other, but the mobile fluid particles cannot displace the matrix particles. Choosing all particles to interact as hard spheres, any state point is fully characterized by a combination of ϕ_m and ϕ_f. Different, but equivalent matrix configurations of a given state point are obtained from an equilibrated hard-sphere fluid at a prescribed ϕ_m. For this, a pertinent simulation is halted at different times and the particle positions are subsequently used as positions of the matrix particles in a QA system. In all MD simulations we have used an event-driven MD algorithm adapted to keeping the matrix particles at fixed positions. Periodic boundary conditions and the minimum image convention were employed.

As prescribed by thermodynamics [24, 34, 35], observables are obtained from a double-averaging procedure: the first trace, taken over the degrees of freedom of the fluid particles for a particular matrix configuration, is realized using a time average along the simulation run; the second one, taken over different yet equivalent matrix configurations, is realized as an ensemble average over independent simulation runs. All state points were studied via ensembles in which the number of fluid particles (N_f) and the number of matrix particles (N_m) added up to at least 1000. For systems with elevated matrix packing fractions this number was considerably enhanced in an effort to guarantee that for all state points considered the ensemble contain at least 50 fluid particles. A method for finding an initial configuration of QA systems at large values of the total packing fraction, $\phi_m + \phi_f$, has been presented and discussed in appendix A of [26].

In the first phase of the simulation the system is equilibrated; for clarifying comments on this delicate issue we refer the reader to section II of [26]. In case the system was successfully brought to equilibrium, we subsequently recorded the particle positions in a production run extending over the same simulation time as the equilibration run. We typically allowed for a maximum of $30\,000\tau$ for the equilibration run;

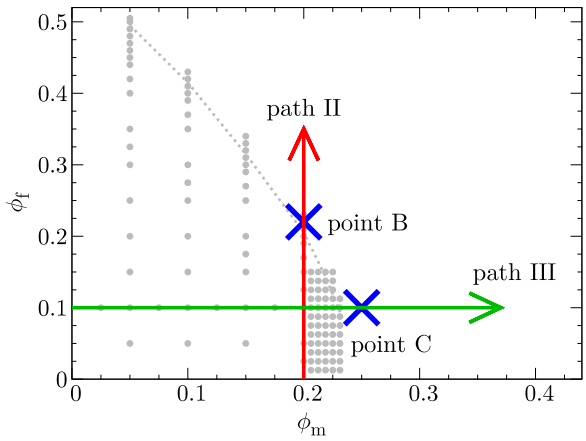

Figure 2. Parameter space for QA systems of hard spheres, spanned by the packing fraction of the matrix particles, ϕ_m, and that of the fluid particles, ϕ_f. The paths and points relevant to this contribution are indicated as large arrows and crosses. For reference, they are superimposed to data taken from figure 4 in [26], in which simulations were performed at state points indicated by the solid circles, and systems right of the dotted line were defined to be 'arrested' based on $F_s(k = 7, t)$.

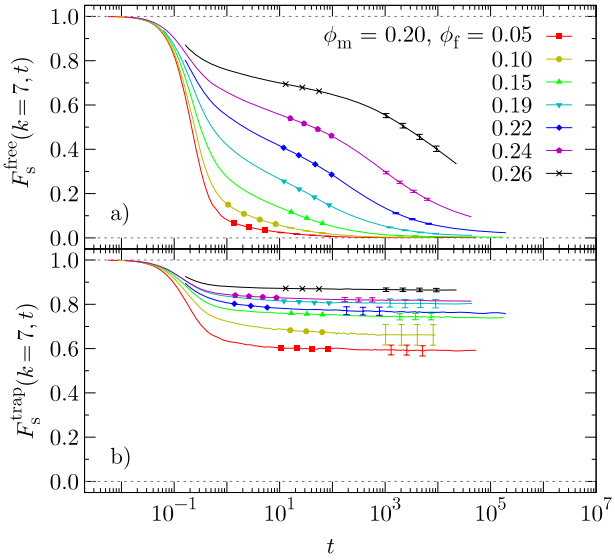

Figure 3. Single-particle intermediate scattering function as a function of time t at fixed $k = 7$ and $\phi_m = 0.20$ for a series of ϕ_f. (a) For the free particles, $F_s^{free}(k, t)$, (b) for the trapped particles, $F_s^{trap}(k, t)$. Error bars represent one standard deviation of the mean for different system realizations.

for selected systems this figure was increased to the tenfold value. Here $\tau = \sqrt{m\sigma^2/k_B T}$ is the unit of time [36], where the particle mass m, the temperature T, and the particle diameter σ were chosen to be unity.

The definitions of all observed quantities presented in this work ($F_s(k, t)$, $\delta r^2(t)$, $z(t)$, and $G_s(r, t)$) have been compiled in [26], to which we refer the reader.

3. Results

3.1. Void analysis

Due to the statistical nature of our matrix model, at any value of the matrix packing fraction ϕ_m there is a nonvanishing probability for the immobile matrix particles to form traps—void spaces from which fluid particles enclosed therein are not able to escape due to geometric restrictions. At low values of ϕ_m the number of traps is small, and most fluid particles can move infinitely far away from their initial location since the void in which they are located extends (taking into account the periodic boundary conditions) over the entire space. The latter volume, if present, is termed the 'percolating' void. At sufficiently high ϕ_m, on the other hand, all voids will be of finite size and represent traps from which the fluid particles cannot escape. The transition between the two scenarios occurs at the so-called percolation transition. (For an overview over the large field of percolation transitions see, e.g. [37].) For an infinitely large system this transition is sharp, i.e. it occurs at some well-defined value ϕ_m^* of the matrix packing fraction. However, if the system is represented by a finite number of particles then this transition is smeared out; for this reason in computer simulations matrix realizations featuring a percolating void are encountered also beyond ϕ_m^*.

We employed an algorithm based on a Delaunay tessellation—details are presented in [33]—in order to identify for a given matrix configuration whether a void constitutes a trap or the percolating void. Using the position of a fluid particle at an arbitrary instance of time, it is thus possible to determine whether the particle in question is 'free' or 'trapped' (according to the previously introduced notion). The method, which has recently received considerable attention in contexts similar to the one of this work [32, 38, 39], is sketched in figure 1.

3.2. Dynamic correlation functions

Making use of the distinction in trapped and free particles, the single-particle correlation functions $F_s(k, t)$, $\delta r^2(t)$, and $G_s(r, t)$ can be split up in an additive way into two component-weighted contributions: one stemming from the N_f^{trap} trapped particles (index 'trap'), the other one from the N_f^{free} free particles (index 'free'). Since the fraction $N_f^{trap}/(N_f^{free} + N_f^{trap})$ increases with ϕ_m, the correlation functions of the trapped particles will suffer from poor statistics at low ϕ_m, whereas for $\phi_m > \phi_m^*$ the results for the correlation functions of the free particles will be affected by a relatively large numerical error.

To facilitate comparison with previous data [25, 26], in this contribution we discuss the results in a similar fashion. This includes the wavevector at which we examine $F_s(k, t)$, namely $k = 7$ (this value is close to the first peak in the structure factor $S(k)$), as well as the choice of specific paths in the parameter space—depicted in figure 2—at which we evaluated $F_s(k, t)$ and $\delta r^2(t)$. Path I in these works (extending at fixed, low ϕ_m while increasing ϕ_f) will not be considered here since trapping—the key property studied in this contribution—plays only a minor role in this region of the kinetic diagram. Path II denotes systems at the intermediate fixed value $\phi_m = 0.2$ and increasing fluid packing fractions; note that the matrix packing fraction along path II is lower than

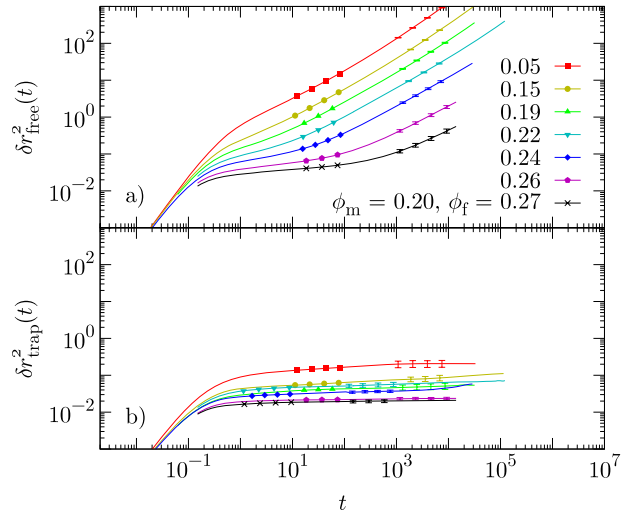

Figure 4. Mean squared displacement as a function of time t at fixed $\phi_{\rm m} = 0.20$ for a series of $\phi_{\rm f}$. (a) For the free particles, $\delta r^2_{\rm free}(t)$, (b) for the trapped particles, $\delta r^2_{\rm trap}(t)$. Error bars: see figure 3.

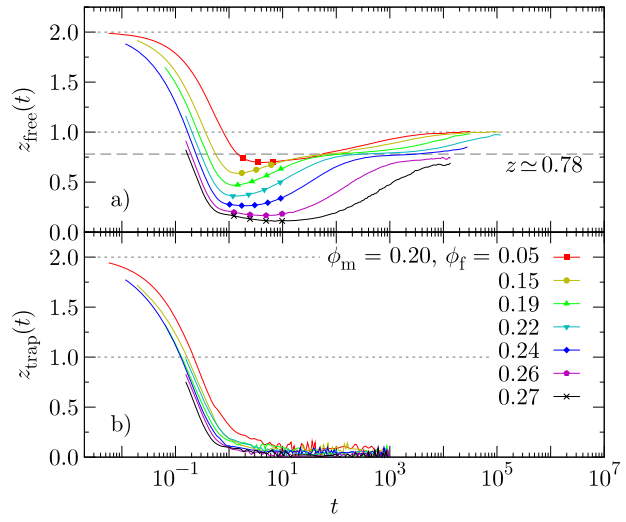

Figure 5. Logarithmic derivative of the mean squared displacement as a function of time t at fixed $\phi_{\rm m} = 0.20$ for a series of $\phi_{\rm f}$. (a) For the free particles, $z_{\rm free}(t)$, (b) for the trapped particles, $z_{\rm trap}(t)$.

the percolation threshold, which has been shown to occur at $\phi^*_{\rm m} = 0.2512$ [25, 26, 33]. Finally, along path III $\phi_{\rm f}$ is kept fixed at 0.1 while increasing $\phi_{\rm f}$ over an interval that includes the percolation transition of the voids at $\phi^*_{\rm m}$.

We start with the discussion of $F_{\rm s}(k,t)$ along path II; the respective contributions of the free and the trapped particles are displayed in figure 3. Essentially, $F^{\rm free}_{\rm s}(k=7,t)$ exhibits the same behaviour as the total correlator, $F_{\rm s}(k{=}7,t)$ (shown in figure 8(b) of [26]), except for the fact that the long-time tail now tends towards zero for all equilibrated samples. In contrast, $F^{\rm trap}_{\rm s}(k{=}7,t)$ shows a long-time plateau that increases with $\phi_{\rm f}$, which can be explained as follows: since we keep the value of $\phi_{\rm m}$ fixed, the void size distribution is the same for all systems along path II. The increase in the plateau is therefore due to the increasing number of trapped fluid particles, which cause mutual jamming effects inside the

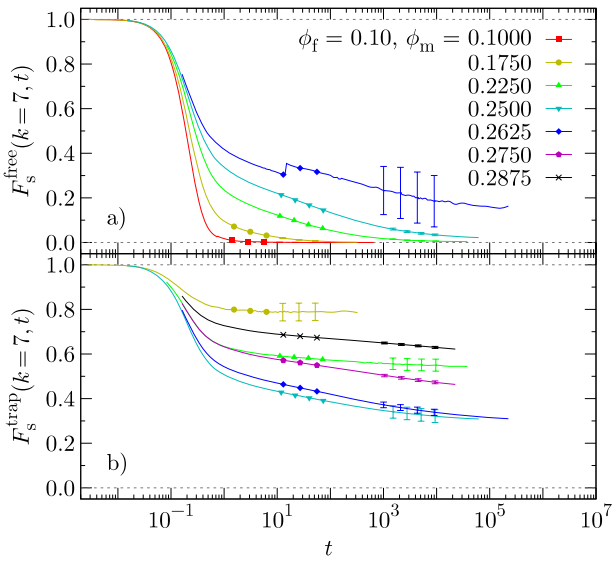

Figure 6. Single-particle intermediate scattering function as a function of time t at fixed $k = 7$ and $\phi_{\rm f} = 0.10$ for a series of $\phi_{\rm m}$. (a) For the free particles, $F^{\rm free}_{\rm s}(k,t)$, (b) for the trapped particles, $F^{\rm trap}_{\rm s}(k,t)$. Error bars: see figure 3.

trapping voids that in turn prevent the correlator from fully relaxing as t tends to infinity.

The consequences of an increasing fluid packing fraction are even more obvious in the respective contributions to the mean squared displacement, $\delta r^2(t)$, displayed in figure 4. In the long-time limit, $\delta r^2_{\rm free}(t)$ shows normal diffusive behaviour for all equilibrated systems. In contrast, in the long-time limit of $\delta r^2_{\rm trap}(t)$ a saturation is observed; the plateau values decrease as $\phi_{\rm f}$ is increased, which is due to the crowding to which the fluid particles are subjected for larger fluid packing fractions. Assuming an instantaneous power-law behaviour $\delta r^2(t) \propto t^z$, the respective long-time behaviour of both contributions to the mean squared displacement is nicely reflected in the subdiffusion exponent $z(t)$, as displayed in figure 5: it quickly drops to zero for the trapped particles, whereas for the free particles $z_{\rm free}(t)$ tends to unity as $t \to \infty$, which corresponds to diffusive behaviour (for the three lowermost curves in figure 5(a) the limit is not approached yet). Notably, for several decades in time an intermediate-time plateau can be observed in $z_{\rm free}(t)$; the value of this plateau is virtually the same as that found for the exponent pertaining to $\delta r^2(t)$ for the full fluid (see figure 9(b) in [26]).

The contributions to $F_{\rm s}(k,t)$ along path III are displayed in figure 6. Disregarding in panel (a) the state point above the percolation threshold (which is poorly equilibrated with respect to the free particles), we find that $F^{\rm free}_{\rm s}(k = 7,t)$ relaxes all the way to zero for $t \to \infty$. This contrasts with the single-particle intermediate scattering function of the full fluid—cf figure 10(b) in [26]—which attains a nonzero long-time plateau that increases with the matrix packing fraction. Hence, the nondecaying part of $F_{\rm s}(k,t)$ must be entirely due to the trapped particles; this fact is reflected in the significant nonrelaxing part of $F^{\rm trap}_{\rm s}(k,t)$. We observe that $F^{\rm trap}_{\rm s}(k,t{\to}\infty)$ exhibits a nonmonotonic behaviour, attaining a minimum value at $\phi_{\rm m} \simeq 0.25$, which is close to the percolation

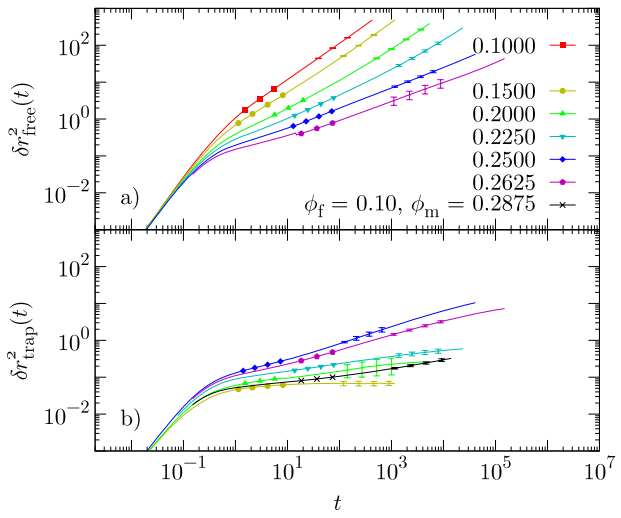

Figure 7. Mean squared displacement as a function of time t at fixed $\phi_{\rm f} = 0.10$ for a series of $\phi_{\rm m}$. (a) For the free particles, $\delta r^2_{\rm free}(t)$, (b) for the trapped particles, $\delta r^2_{\rm trap}(t)$. Error bars: see figure 3.

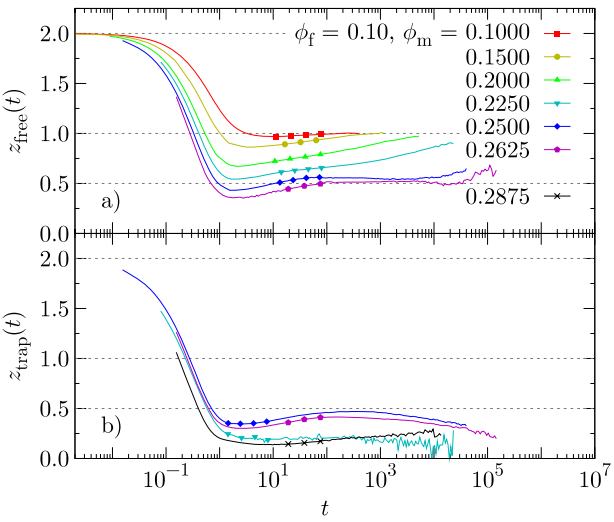

Figure 8. Logarithmic derivative of the mean squared displacement as a function of time t at fixed $\phi_{\rm f} = 0.10$ for a series of $\phi_{\rm m}$. (a) For the free particles, $z_{\rm free}(t)$, (b) for the trapped particles, $z_{\rm trap}(t)$.

transition in the void space [33]. $\delta r^2_{\rm free}(t)$ and $z_{\rm free}(t)$—the latter presented in figure 8—show features similar to those of their equivalents for the full fluid (cf figure 11 in [26]), apart from two differences. Firstly, $z_{\rm free}(t)$ shows an onset to recover diffusive behaviour for $\phi_{\rm m} = 0.2625$, as opposed to $z(t)$ which shows a trend to saturation. Therefore, in the time range in question ($t \simeq 10^5$) the mean squared displacement of the full fluid has to be dominated by the contribution of the trapped particles. The second interesting feature is the much clearer subdiffusive regime for $\phi_{\rm m} = 0.2625$, which now remains at an essentially invariable $z_{\rm free} \simeq 0.5$ for almost three decades in time. The mean squared displacement of the trapped particles reveals a similarly interesting behaviour: while $\delta r^2_{\rm trap}(t)$, shown in figure 7, is subdiffusive with $z_{\rm trap}(t) < 0.5$ at all times, for matrix packing fractions close to the percolation threshold $z_{\rm trap}(t)$ attains much larger values of almost 0.5 at intermediate times, and $\delta r^2_{\rm trap}(t)$ saturates at much larger values in this $\phi_{\rm m}$ regime. The latter indicates that the average trap size attains a maximum at $\phi^*_{\rm m}$. This behaviour is well known from percolation theory, which predicts the average trap size to diverge; onsets of this phenomenon were also shown to exist in [33, 32].

The self-part of the direction-averaged van Hove function, $G_{\rm s}(r, t)$, shall be discussed for two selected state points, labelled point 'B' and point 'C', which are indicated in figure 2. Point B is located on path II (fixed $\phi_{\rm m} = 0.20$) at a fluid packing fraction $\phi_{\rm f} = 0.22$, where the latter value has been shown sufficient to cause a relatively slow relaxation of the fluid's dynamic features [25, 26]. The respective contributions to the van Hove functions are depicted in figure 9. The main peak of $G^{\rm free}_{\rm s}(r, t)$ at small distances drops rapidly at small times. However, for large times it is still present; this is probably due to fluid particles that are located at the end of long, narrow dead-end channels like the one schematically drawn in figure 10. Those channels are connected to the percolating void, but very improbable collective rearrangements would have to occur for the end-particle to leave its position. At intermediate times and $r \sim 1.1$ we see a pronounced peak in $G^{\rm free}_{\rm s}(r, t)$, which indicates hopping processes of the free particles. $G^{\rm trap}_{\rm s}(r, t)$, on the other hand, quickly reaches a stationary distribution; the latter is relatively narrow, which indicates that for $\phi_{\rm m} = 0.20$ only a small fraction of pores is large enough to accommodate more than one particle. For large times the van Hove function displays a small shoulder at $r \sim 0.5$, reflecting the pore size distribution; the small peak at $r \sim 1$ emerging for large times evidences that despite the small average trap size there exist traps large enough for particles to collectively rearrange.

Point C, the other point at which we examined $G_{\rm s}(r, t)$, is located on path III and is characterized by $\phi_{\rm f} = 0.1$ and $\phi_{\rm m} = 0.25$; notably, the latter figure is close to the percolation threshold. The respective contributions to the van Hove functions are depicted in figure 11. The main peak of $G^{\rm free}_{\rm s}(r, t)$ at $r \sim 0$ drops to zero as t tends to infinity. For $r = 0$ a minute peak seems to persist; it might be associated with the trapping phenomena discussed in section 4. Other than a hopping peak at $r \sim 1$ (less pronounced than that in figure 9) there are no unusual features in $G^{\rm free}_{\rm s}(r, t)$. In contrast, for this state point $G^{\rm trap}_{\rm s}(r, t)$ shows a behaviour which is distinctively different from that of the same correlator for the other state point: at point C the evolution of the stationary state at $t \to \infty$ takes considerably more time than at point B (cf figure 9). Also, the pronounced peak at small distances in the limiting function evidences a considerable amount of trapping; the broad side peak at $r \sim 1.1$ reflects hopping processes inside the traps. Finally, it is worth noting that $G^{\rm trap}_{\rm s}(r, t \to \infty)$ exhibits a very long tail in r; this is another indication of the fact that close to the percolation transition there exist very large traps.

4. Discussion

Our analysis of the dynamic correlation functions for the free and the trapped particles provides some deeper insight

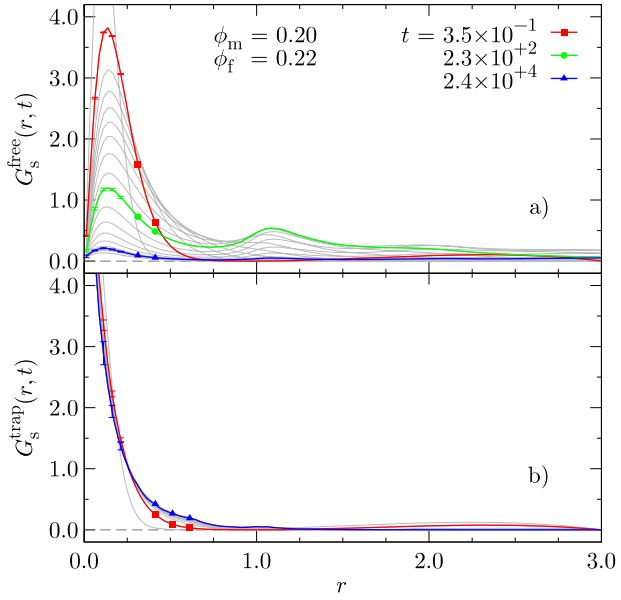

Figure 9. Self-part of the direction-averaged van Hove function as a function of r at point 'B', defined via $\phi_m = 0.20$ and $\phi_f = 0.22$. (a) For the free particles, $G_s^{free}(r,t)$, (b) for the trapped particles, $G_s^{trap}(r,t)$. Curves are approximately logarithmically spaced in time; some are highlighted for visual guidance. Error bars: see figure 3.

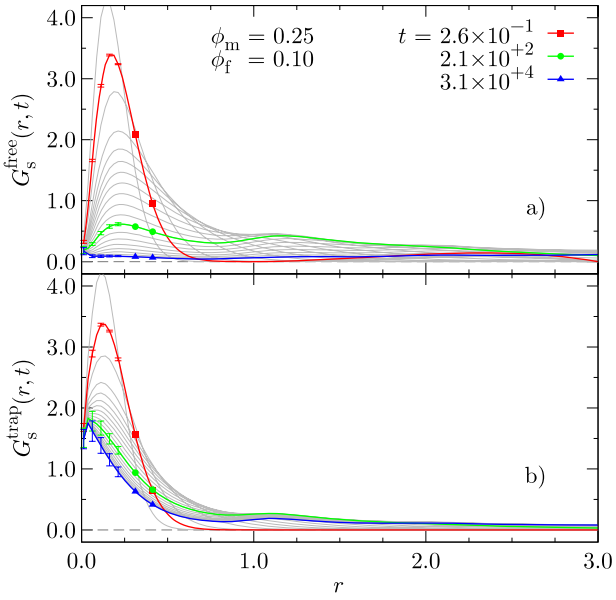

Figure 11. Self-part of the direction-averaged van Hove function as a function of r at point 'C', defined via $\phi_m = 0.25$ and $\phi_f = 0.10$. (a) For the free particles, $G_s^{free}(r,t)$, (b) for the trapped particles, $G_s^{trap}(r,t)$. Curves are approximately logarithmically spaced in time; some are highlighted for visual guidance. Error bars: see figure 3.

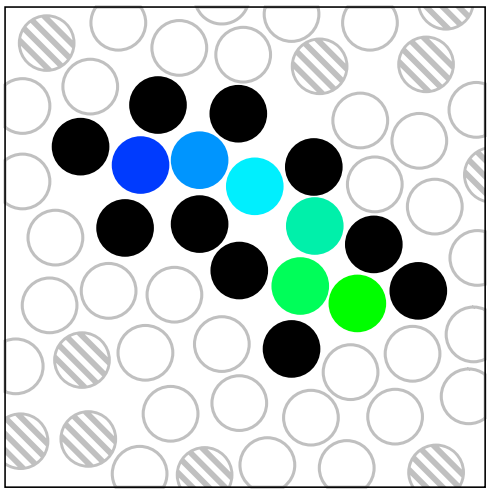

Figure 10. Two-dimensional schematic of a long dead-end channel. Black solid circles: matrix particles that form the dead-end channel. Grey (coloured) solid circles: fluid particles in the channel. Light (grey) hatched circles: other matrix particles. Light (grey) open circles: other fluid particles. From light (green) to medium (blue) there is a decreasing probability for the respective particle to leave its position via collective rearrangements.

into the complex relaxation of a colloidal fluid adsorbed in a dense immobile matrix. Comparison with results for the full fluid [25, 26] strengthens our previous interpretation of the dynamic data and allows to assess the various predictions of MCT [20–22] from a broader perspective:

(i) The complex relaxation of the single-particle correlators, along a pathway representative of the behaviour at intermediate matrix and large fluid densities (path II), arises from a genuine superposition of trapping effects and a collective caging mechanism; the former leads to a finite long-time plateau in $F_s(k,t)$, while the latter is responsible for the inflection in the intermediate-time regime of this correlation function. This observation strongly supports our previous interpretation for the data of the full fluid along this path [25, 26] and indicates that this behaviour may correspond, at least on a qualitative level, to the crossing of the two arrest lines (diffusion–localization and glass transition) as predicted by MCT.

(ii) The values of the subdiffusion exponent z for the full fluid [25, 26] clearly show that the free fluid particles undergo a subdiffusive process on their own right. Moreover, the values of z for the full fluid are only marginally affected by the contribution of the trapped particles: our calculation of z_{free} at a packing fraction close to the estimated percolation transition is, within error margin, indistinguishable from the value 0.5 found in the full system. As an observational fact, the same value of z is featured in single-file diffusion [40, 41] and is also predicted by MCT along the diffusion–localization transition [22]. However, it is well known that MCT cannot properly describe the diffusion of a tracer particle in a disordered frozen matrix such as in the Lorentz gas model [22, 42]. In particular, in the Lorentz gas the subdiffusion exponent $z = 0.32$ is observed at the percolation transition [29, 30], which differs from the value $z = 0.5$ predicted by MCT at the diffusion–localization transition in QA systems. Motivated by this observation and by related findings in previous works [27, 43], we have examined the case of non-interacting tracer particles moving in a QA-type matrix at

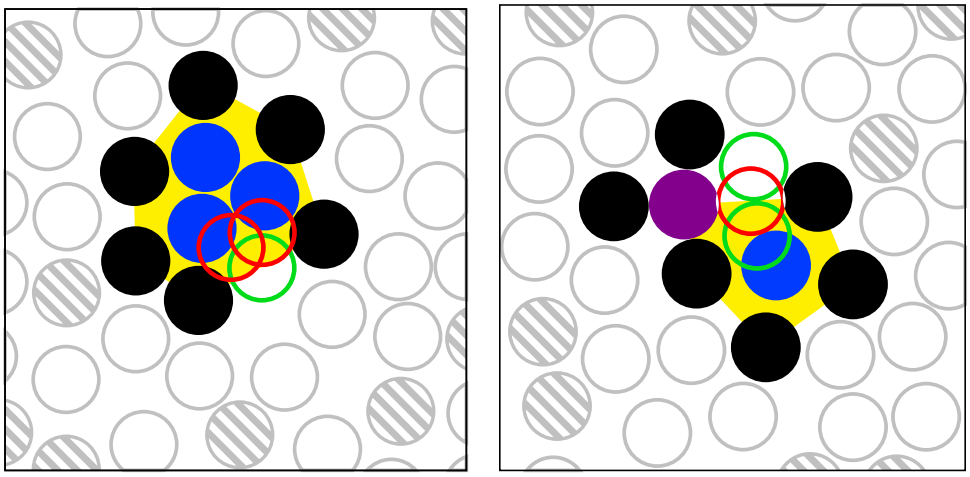

Figure 12. Two-dimensional schematics for mechanisms of effective trapping, induced by the presence of multiple fluid particles in the system. Black solid circles: relevant matrix particles. Dark (purple) solid circles: trapped particles. Medium-shade (blue) solid circles: effectively trapped particles. Light (green) open circles: positions a fluid particle can occupy. Medium-shade (red) open circles: positions a fluid particle cannot occupy due to overlaps. Light (yellow): area constituting the effective trap. Light (grey) hatched circles: other matrix particles. Light (grey) open circles: other fluid particles populating the percolating void. (a) The effectively trapped particles are located in a pore connected to the percolating void; however, due to jamming the particles cannot rearrange such that one of them would reach the connecting channel. (b) The effectively trapped particles are located in a pore connected to the percolating void; however, another fluid particle (dark (purple)) is trapped between matrix particles in a way that it blocks the connecting channel for the particles in the pore (medium-shade (blue)).

the percolation transition [44]. We found that in this case z for the full fluid assumes a value around 0.3, which is more similar to the value found in the Lorentz gas than to the value predicted by MCT. The apparent disagreement between the case of non-interacting tracers and the case of a dense fluid moving in such matrices will be subject to future work [44].

(iii) The splitting procedure effectively removes the nonzero long-time limit of $F_s(k,t)$. This method therefore provides a microscopic basis to the empirical procedure described in [26], where an *ad hoc* subtraction of the long-time plateau was performed. The agreement between the results of the two procedures (not discussed here) lends support to our discussion of the modified kinetic diagram for single-particle properties presented in [26].

Even more intriguing is the observation of nontrivial dynamic heterogeneity in both the trapped and the free component of the fluid particles. For the free particles, the van Hove function displayed in figure 11(a) evidences that a non-negligible fraction of the particles undergo a very slow relaxation. At least three physical mechanisms explaining this finding can be identified. (i) Free particles may be located at the end of long dead-end channels as shown in figure 10; the longer such a channel is, the less likely are the collective rearrangements required for a particle to escape from the channel's end. (ii) Free particles may mutually jam in a pore as schematized in figure 12(a); such particles are rigorously confined to that pore since none of them can reach the channel that connects the pore to the percolating void. (iii) A trapped particle may act as an 'effective' matrix particle (see figure 12(b)); if the matrix restricts its movement to much less than its radius, it can block a pathway in the percolating void; this may render the void at one side of that pathway a trap. Visual inspection of animated trajectories of our systems confirmed that all of these processes are present and relevant in the portion of the kinetic diagram corresponding to large ϕ_f and ϕ_m. Note that effects (ii) and (iii) arise from the QA-protocol requirement that all available volume (including traps) be populated with fluid particles.

Notably, dynamic heterogeneity is also present among the trapped particles; they have been observed to rearrange collectively for instance by exchanging their positions in a closed loop. Thus, for the trapped particles an apparent weak relaxation appears in the single-particle correlators and a tail emerges at large distances in their van Hove function. A more systematic analysis of these striking dynamic features is currently underway.

5. Conclusions

We have presented a computational study concerned with the dynamic properties of a model colloidal fluid adsorbed in a disordered, rigid array of obstacles. The original aspect of this study consists in the splitting of dynamic correlators into two contributions, one originating from the free and the other from the trapped fluid particles. The notion of 'free' and 'trapped' refers to the structure of the voids formed by the matrix: free particles are located in the infinitely large percolating void whereas trapped particles reside in disconnected voids. We compared the relaxation patterns of the two components with the corresponding patterns for the full fluid, which allows to disentangle the dynamic effects due

to crowding and confinement. Further, our procedure provides some deeper insight into the relaxation processes at play at the microscopic level. Our analysis confirmed the striking superposition of two relaxation mechanisms—trapping and caging—at a sufficiently large density of both the fluid and the matrix component, and supported the view that MCT correctly captures the qualitative features of the dynamics in the corresponding portion of the kinetic diagram. Our numerical procedure also unveils that an unexpected dynamic heterogeneity is present in the motion of fluid particles within the matrix structure: on the one hand, even particles residing in a percolating void may be effectively trapped; on the other hand, residual relaxation can take place within disconnected pores. We believe these aspects to be relevant also for the assessment of dynamic heterogeneity in more general models of fluids adsorbed in porous media. Whether these complex dynamic phenomena are present also in systems with different protocols to generate the matrix [27, 45], soft interactions [25], or systems in which a large dynamic asymmetry replaces the quenched disorder [46, 47, 43] is a question that remains to be addressed in future studies.

Acknowledgments

We acknowledge fruitful discussions with V Krakoviack and T Franosch. This work was financially supported by the Austrian Research Fund (FWF) under Proj. Nos P19890-N16 and W004.

References

[1] Gelb L D, Gubbins K E, Radhakrishnan R and Sliwinska-Bartkowiak M 1999 *Rep. Prog. Phys.* **62** 1573
[2] Rosinberg M L 1999 *New Approaches to Problems in Liquid State Theory* ed C Caccamo, J P Hansen and G Stell (Dordrecht: Kluwer Academic)
[3] McKenna G B 2000 *J. Physique* IV **10** 343
[4] McKenna G B 2003 *Eur. Phys. J.* E **12** 191
[5] Alcoutlabi M and McKenna G B 2005 *J. Phys.: Condens. Matter* **17** R461
[6] McKenna G B 2007 *Eur. Phys. J. Spec. Top.* **141** 291
[7] Lomba E, Given J A, Stell G, Weis J J and Levesque D 1993 *Phys. Rev.* E **48** 233
[8] Vega C, Kaminsky R D and Monson P A 1993 *J. Chem. Phys.* **99** 3003
[9] Meroni A, Levesque D and Weis J J 1996 *J. Chem. Phys.* **105** 1101
[10] Paschinger E and Kahl G 2000 *Phys. Rev.* E **61** 5330
[11] Rosinberg M L, Tarjus G and Stell G 1994 *J. Chem. Phys.* **100** 5172
[12] Kierlik E, Rosinberg M L, Tarjus G and Monson P 1995 *J. Chem. Phys.* **103** 4256
[13] Kierlik E, Rosinberg M L, Tarjus G and Monson P A 1997 *J. Chem. Phys.* **106** 264
[14] Álvarez M, Levesque D and Weis J J 1999 *Phys. Rev.* E **60** 5495
[15] Paschinger E, Levesque D, Kahl G and Weis J J 2001 *Europhys. Lett.* **55** 178
[16] Gallo P, Pellarin R and Rovere M 2003 *Phys. Rev.* E **67** 041202
[17] Kim K 2003 *Europhys. Lett.* **61** 790
[18] Chang R, Jagannathan K and Yethiraj A 2004 *Phys. Rev.* E **69** 051101
[19] Mittal J, Errington J R and Truskett T M 2006 *J. Phys. Chem.* B **110** 18147
[20] Krakoviack V 2005 *Phys. Rev. Lett.* **94** 065703
[21] Krakoviack V 2007 *Phys. Rev.* E **75** 031503
[22] Krakoviack V 2009 *Phys. Rev.* E **79** 061501
[23] Gotze W and Sjogren L 1992 *Rep. Prog. Phys.* **55** 241
[24] Given J A and Stell G R 1994 *Physica* A **209** 495
[25] Kurzidim J, Coslovich D and Kahl G 2009 *Phys. Rev. Lett.* **103** 138303
[26] Kurzidim J, Coslovich D and Kahl G 2010 *Phys. Rev.* E **82** 041505
[27] Kim K, Miyazaki K and Saito S 2009 *Europhys. Lett.* **88** 36002
[28] Gallo P, Attili A and Rovere M 2009 *Phys. Rev.* E **80** 061502
[29] Höfling F, Franosch T and Frey E 2006 *Phys. Rev. Lett.* **96** 165901
[30] Höfling F and Franosch T 2007 *Phys. Rev. Lett.* **98** 140601
[31] Babu S, Gimel J C and Nicolai T 2008 *J. Phys. Chem.* B **112** 743
[32] Sung B J and Yethiraj A 2008 *J. Chem. Phys.* **128** 054702
[33] Kurzidim J and Kahl G 2011 **109** 1331
[34] Given J A 1992 *Phys. Rev.* A **45** 816
[35] Given J A and Stell G 1992 *J. Chem. Phys.* **97** 4573
[36] Allen M P and Tildesley D J 1987 *Computer Simulation of Liquids* (Oxford: Oxford University Press)
[37] Stauffer D and Aharony A 1995 *Perkolationstheorie: eine Einführung* (Weinheim: VCH)
[38] Spanner M, Höfling F, Schröder-Turk G, Mecke K and Franosch T 2011 *J. Phys.: Condens. Matter* **23** 234120
[39] Kim K, Miyazaki K and Saito S 2011 *J. Phys.: Condens. Matter* **23** 234123
[40] Kärger J 1992 *Phys. Rev.* A **45** 4173
[41] Wei Q H, Bechinger C and Leiderer P 2000 *Science* **287** 625
[42] Schnyder S K, Höfling F, Franosch T and Voigtmann T 2011 *J. Phys.: Condens. Matter* **23** 234121
[43] Voigtmann T and Horbach J 2009 *Phys. Rev. Lett.* **103** 205901
[44] Kurzidim J and Kahl G 2011 unpublished
[45] Krakoviack V 2010 *Phys. Rev.* E **82** 061501
[46] Moreno A J and Colmenero J 2006 *Phys. Rev.* E **74** 021409
[47] Fenz W, Mryglod I M, Prytula O and Folk R 2009 *Phys. Rev.* E **80** 021202